JOURNAL OF THERMOPHYSICS AND HEAT TRANSFER
Vol. 13, No. 4, October-December 1999

Aircraft Skin-Cooling System for Thermal Management of Onboard High-Power Electronics

Ab Hashemi*
Lockheed Martin Missiles and Space, Palo Alto, California 94304-1191
Elizabeth Dyson†
Lockheed Martin Canada, Kanata, Ontario K2K 2M8, Canada
and
Jay Nigen‡
Innovative Research, Inc., Minneapolis, Minnesota 55413

Integration of high-power electronic devices into existing aircraft, while minimizing the impact of additional heat load on the environmental control system of the aircraft, requires innovative approaches. One such approach is to reject heat through the aircraft skin by use of internal skin ducts with enhanced surfaces. This approach requires a system-level consideration of the effect of cooling ducts, inlets, and outlets on the performance of the electronic equipment and effectiveness of the heat rejection system. The development of a system-level model to evaluate the performance of electronic equipment in an aircraft cabin and heat rejection through the skin is described. The outer surface of the fuselage is treated as a heat exchanger. Hot air from an equipment exhaust plenum is drawn into a series of baffled ducts within the fuselage support structure, where the heat is rejected and then recirculated into the cabin. The cooler air from the cabin is then drawn into the electronic equipment. The aircraft air conditioning unit is also modeled to provide chilled air directly into the cabin. Also, a series of tests is described, which were performed to verify the model assumptions for heat dissipation from and airflow through the equipment. The tests were performed using the actual electronic equipment in a representative cabin configuration. Results indicate very good agreement between the analytical calculations for the design point and model predictions.

Nomenclature

A = flow area
C = heat loss coefficient
c_p = specific heat at constant pressure
c_v = specific heat at constant volume
D_h = hydraulic diameter
$F(\dot{Q})$ = driving force function
f = Darcy friction factor
Gr = Grashoff number
H = enthalpy
$\dot{H}$ = enthalpy generation
h = heat transfer coefficient
K = minor loss coefficient
k = thermal conductivity
L = length
$L(\dot{Q})$ = flow resistance function
M = Mach number
m = mass
$\mathring{m}$, $\dot{M}$ = mass flow rate
Nu = Nusselt number
P = perimeter
Pr = Prandtl number
p = pressure
Q_s = solar constant
$\dot{Q}$ = volumetric flow rate
q = heat flux
R = universal gas constant
Re = Reynolds number
$\dot{S}$ = enthalpy input
s = distance from the nose of the aircraft
T = temperature
T^* = recovery temperature
t = time
U = overall heat transfer coefficient
$\mathcal{V}$ = volume
$\boldsymbol{v}$ = velocity vector
$\dot{W}$ = work input
α_s = surface solar absorptivity
γ = specific heat ratio, c_p/c_v
ΔT = temperature difference
ε_{wo} = surface emissivity
μ = viscosity
ξ = beginning of heated section
ρ = density
σ = Stefan–Boltzman constant
τ = shear stress
$\tau(\dot{Q})$ = viscous loss function

Subscripts

a = ambient
b = bulk
CF = coefficient for driving force source term
CR = coefficient for flow resistance term
e = external
I = node number or internal
ij = link number
k = link index
s = local
skin = aircraft heat rejection surface
wi = skin internal surface
wo = skin external surface
∞ = far-field temperature

Received 13 March 1998; revision received 9 February 1999; accepted for publication 11 February 1999.

*Consulting Engineer and Thermal Sciences Manager, Advanced Technology Center.
†Senior Systems Engineer; currently Senior Project Director, SHL Systemhouse Co., Hull, Quebec J8X 4B7, Canada.
‡Engineer; currently Engineer, Electronics Industry Team, Fluent, Inc., 3255 Kifer Road, Santa Clara, CA 95051.

Introduction

RETROFITTING of military and commercial aircraft with high-power electronic equipment provides additional heat source in the cabin. The existing aircraft environmental control system cannot handle the additional heat load created by this electronic equipment; thus the aircraft requires supplemental cooling to fulfill its mission.

To overcome this heat rejection limitation in a CL-600 Challenger aircraft, a skin-cooling design has been developed. The design is fully described by Dyson et al.[1] and Hashemi et al.[2,3] The concept calls for baffled ducts at the aircraft skin to cool the air in the aft cabin, where the equipment is located. The hot air from the rack with the equipment that dissipates the most heat is exhausted into a plenum that connects to a ceiling duct, from which it is distributed by fans into the baffled ducts. These ducts, which are bounded by the cold skin on one side, are used as a heat exchanger to reject the heat. The cooled air is then recirculated into the aft cabin.

The heat transfer coefficient and the pressure drop in the skin-cooling ducts were estimated using two-dimensional[4] and three-dimensional[1–3] computational fluid dynamics (CFD) models developed for this program. These models include conjugate heat transfer and turbulence models and consider convection and radiation exchange between the aircraft and its surroundings. The three-dimensional model predictions were verified by laboratory experiments on a representative section of the skin-cooling duct.[1–3] Based on analytical models and experimental data, the aft cabin temperature was calculated and presented by Dyson et al.[1] and Hashemi et al.[2,3]

This paper describes the development of a system network model to evaluate the performance of electronic equipment in the aft cabin and heat rejection through the skin. The heat transfer and airflow throughout the entire supplementary cooling system are modeled, and the interaction between the ceiling and equipment fans is included. The model is to serve as a simulation tool for design and off-design prediction of temperature and pressure fields in the aft cabin.

In addition, this paper describes a series of tests that were performed to verify the model assumptions for heat dissipation from and airflow through the equipment. The tests were performed using the actual electronic equipment in a representative cabin configuration. Results indicate good agreement between the test data and equipment specifications for overall heat dissipation and airflow.

Configuration

The general layout of the Challenger aircraft and an overview of the sources of heat dissipation in the aft cabin are fully described by Dyson et al.[1] and Hashemi et al.[2,3] However, for completeness, the important features of the layout are presented in this paper. A schematic of the compartments for the Challenger aircraft is shown in Fig. 1. The aircraft is split into three main areas: the cockpit, the main cabin area, and the aft cabin area, which is the location of most of the high-power electronic equipment and the skin-cooling surface area. The electronic equipment located in the aft cabin area is placed in three equipment racks EW1, EW2, and EW3. The specifications for each piece of equipment in the racks are summarized by Dyson et al.[1] and Hashemi et al.[5]

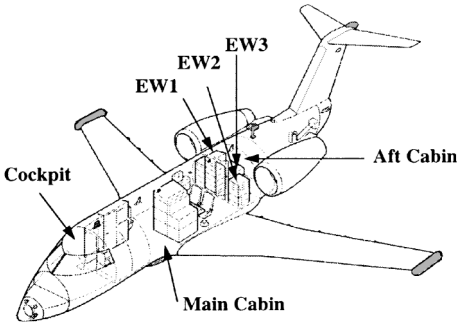

Fig. 1 Challenger cabin layout.

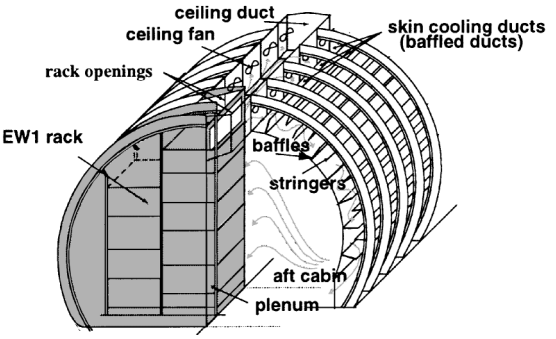

Fig. 2 Aft cabin airflow distribution.

The total possible equipment heat load in the aft cabin exceeds 15 kW. However, the mission scenario provided by Hashemi et al.[5] indicates that the equipment, in a worst-case operational scenario, would dissipate a maximum heat load of 11.7 kW in the aft cabin. This heat must be then rejected to the environment by the supplementary cooling system through the skin of the aircraft.

A schematic of the aircraft supplementary cooling system and air paths is shown in Fig. 2. In this design, baffled ducts at the aircraft skin are used to cool the air in the aft cabin, where the equipment is located. The hot air from the rack with the equipment that dissipates the most heat (EW1) is exhausted into a plenum that connects to a ceiling duct, from which it is distributed by 11 fans into the baffled ducts. These ducts, which are bounded by the cold skin on one side, are used as a heat exchanger to reject the heat. The cooled air is then recirculated into the aft cabin.

The baffles contained within the skin ducts increase mixing and improve overall heat transfer at the cost of increased pressure drop. In addition to the heat transfer provided by the ducts, a limited amount of chilled air is provided directly to the aft cabin from the aircraft air conditioning unit (ACU).

The design point chosen for the skin cooling is International Standard Atmosphere (ISA) +20°C day at 25,000 ft at Mach 0.7. A design goal of 104°F (40°C) for the aft cabin temperature was established based on the lowest common denominator among the equipment recommended inlet temperatures.

Network Model

To predict flow and heat transfer in the aft cabin, a network model was developed using MacroFlow.[6] The model was then used to predict the performance of the aft cabin supplementary cooling system. MacroFlow network models are based on link–node representation. In this representation, each component or subcomponent was modeled by a series of links and nodes. The various combinations of links and nodes were then joined to form the complete system.

Links represent paths along which mass or energy flows. For example, the skin duct is represented by a link. The average cross-sectional area, length, and flow resistance along each link are specified. The link resistance characteristics, in effect, replace the viscous diffusion terms that are lost through spatial averaging. Usually, flow resistance will consist of a functional relationship between the pressure drop and flow rate. This relationship for the baffled ducts was determined through detailed CFD analyses and verified experimentally.[1–3] In addition to flow resistance, links also have finite volumes to account for any inertia associated with the fluid (storage of momentum). In this model, link volumes are assumed to remain unchanged with respect to time. Finally, heat transfer with the environment can occur along a link and is accounted for through the specification of a heat transfer coefficient and exposed surface area.

Nodes represent locations within the system at which pressure, temperature, and fluid properties are determined. A node can represent a reservoir, such as the aft cabin. As with links, heat transfer with the environment can occur at a node and is accounted for through the specification of a heat transfer coefficient and exposed surface area. Therefore, nodes require the specification of exposed surface

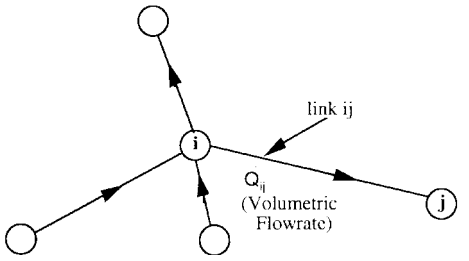

Fig. 3 Generic link-node representation.

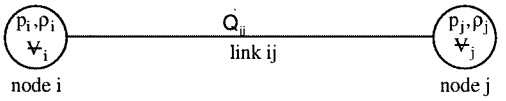

Fig. 4 Generic link-node representation for conservation of momentum.

area and volume, which can be a function of time, as well as initial guesses for density, temperature, and pressure. In this model, only steady-state conditions were considered.

The general governing differential equations employed in MacroFlow are briefly described here. A detailed description of MacroFlow is presented in Ref. 6.

Conservation of mass is applied at each internal node. Figure 3 shows a generic link–node representation, where link ij connects node i to node j. Referring to Fig. 3, the mass balance equation for node i can be represented as

$$\sum_{k=1}^{n_{ij}} (\rho_{ij} \dot{Q}_{ij})_k + \dot{M}_i = 0 \tag{1}$$

The first term represents the sum of mass flux entering the node from all connecting links (1–n_{ij}). Note that a single node can have many connecting links. The second term accounts for any sources or sinks of mass located at node i.

Momentum conservation is formulated at each link because the flow rate is associated with links, not nodes. A generic link is shown in Fig. 4. Although multiple links can connect to a single node, only two nodes can connect to a single link.

The conservation of momentum may be expressed as

$$\rho_{ij} \dot{Q}_{ij} (\boldsymbol{v}_i - \boldsymbol{v}_j) + \Delta p A_{ij} - L(\dot{Q}_{ij}) + \sum_{f=1}^{n_f} F_f(\dot{Q}_{ij}) A_{ij} = 0 \tag{2}$$

The first term represents the convection of momentum into (out of) the link. This term accounts for the change in momentum associated with the acceleration (deceleration) of fluid within the link. Physically, this term has meaning if the area at the entrance of the link was larger (smaller) than that of the exit. The second term represents the net pressure force that is driving the fluid within the link. The third term accounts for losses associated with any flow resistance. Such flow resistance includes viscous losses (shear) and minor losses associated with any elbows, valves, nozzles, etc., within the link, i.e.,

$$L(\dot{Q}_{ij}) = \tau_{ij}(\dot{Q}_{ij}) P_{ij} L_{ij} + \sum_{n=1}^{N} \left(\frac{K \rho_{ij} \dot{Q}_{ij}^2}{2 A_{ij}} \right) \tag{2a}$$

The final term in Eq. (2) represents the total additional driving force provided by any fans within the link. Both the flow losses and additional driving force terms can be linear or nonlinear functions of the flow rate.

As with mass conservation, energy conservation is expressed at each node (Fig. 3). Rather than formulating conservation of energy with temperature as the primary variable, enthalpy is selected so as to remove any difficulties associated with variable specific heat:

$$\sum_{k=1}^{n_{ij}} (\rho_{ij} \dot{Q}_{ij} H_{ij})_k + \dot{S}_i + \dot{W}_i = 0 \tag{3}$$

where the first term represents the net convection of enthalpy into node i through all connected links. The second term represents any enthalpy input to node i that is not associated with transport through the connected links. This cans either be local enthalpy generation or enthalpy transport with the environment, i.e.,

$$\dot{S}_i = \dot{H} + C_i (H_\infty - H_i) \tag{4}$$

For constant specific heat, the coefficient C_i represents the product of the heat transfer coefficient and the exposed surface area, divided by the specific heat, while the enthalpy of the environment is simply the product of the environmental temperature and its specific heat. The final term represents the contribution due to work. Work input is mechanical energy that is added at node i.

The final physical principal that is incorporated in MacroFlow is the relationship between local enthalpy, pressure, and density, i.e., equation of state. In this analysis, the ideal gas law

$$p_i = R(H_i / c_{pi}) \rho_i \tag{5}$$

was used.

The network was assumed to be an open loop, where pressure and enthalpy are known at the inlet boundary. The flow enters and leaves the system through the links associated with the boundary nodes and, as such, provides a relative basis from which pressure and enthalpy are defined. Further, mass conservation is not solved at boundary nodes because they represent the environment.

The discretization of the mass, momentum, and energy equations and their solution are described in Ref. 6. It is noted that the particular computational procedure employed in MacroFlow is similar to the SIMPL algorithm.[7]

Aft Cabin Network Model

The network representation of the cooling configuration for the aft cabin is shown in Figs. 5a–5d. In Figs. 5a–5d, the numbers in the circles are node numbers in the model, and the numbers beside the lines are link numbers. Node 1 (Fig. 5a) represents the intake to the equipment in the EW1 rack. Links 1–10 (Fig. 5b) correspond to the EW1 equipment, chassis 1–10, respectively. Chilled air from the ACU is combined with the aft cabin air at node 65. The heated air exiting the EW1 rack (node 28 in Figs. 5a and 5b) flows to the rack plenum, node 66, and is then drawn into the skin duct by the fans (Fig. 5c). The skin ducts all feed back into the cabin at node 65. Nodes 69 and 105 correspond to the inlet to and exit from the EW2 rack, whereas nodes 70 and 90 correspond to the inlet to and exit from the EW3 rack. The air heated within the EW2 rack returns to the aft cabin at node 65, and the heated air from the EW3 rack partially exits the cabin at node 67. Nodes 91 and 92 correspond to the cabin outlet and inlet environment, and node 93 represents the ACU.

In the aft cabin network model, it was assumed that the flow was steady and incompressible. Air was assumed to behave as an ideal gas, and an open boundary node was assumed, i.e., at least one boundary node with known pressure and enthalpy. Surfaces, lengths, areas, and volumes were estimated based on the best available data and continuously updated, as new information became available. Equipment specifications, i.e., pressure drop, heat dissipation, airflow rate, etc., were obtained from the manufacturer and incorporated into the model. Correlation for the pressure drop and heat transfer in the skin ducts were derived from the CFD calculations.[1–3]

Heat Transfer

The internal convective heat transfer coefficient in the baffled portion of the cooling duct was calculated as a function of mass flow rate using CFD analysis[1–3] from the following equations:

$$h_i = q/(T_b - T_{\text{wi}}) \tag{6}$$

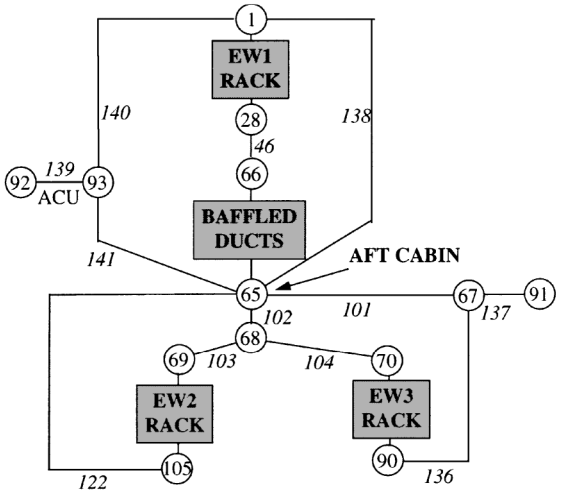

Fig. 5a Link-node representation of the aft cabin.

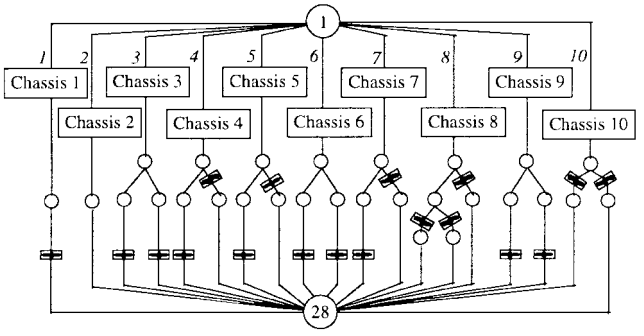

Fig. 5b Link-node representation of the EW1 rack.

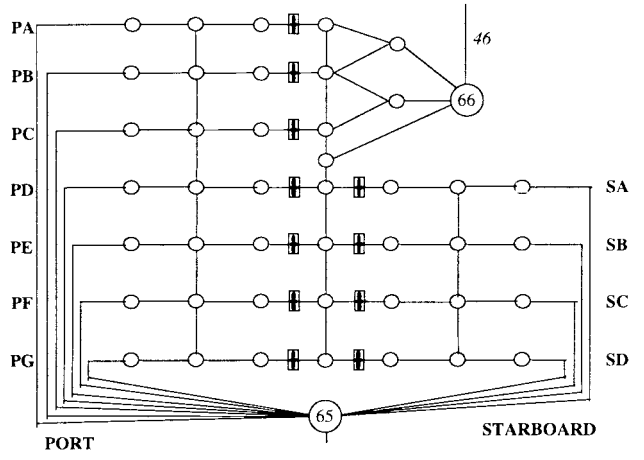

Fig. 5c Link-node representation of the baffled ducts.

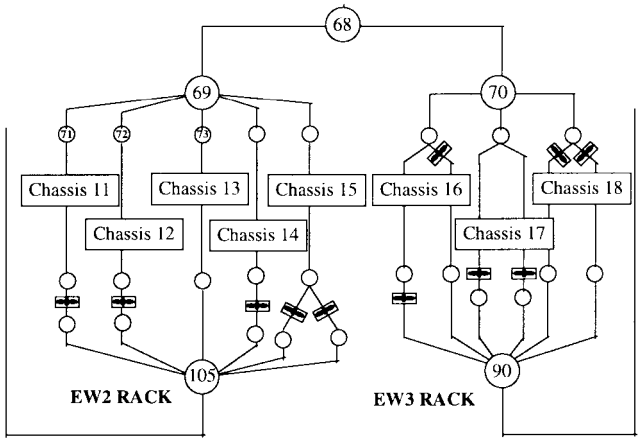

Fig. 5d Link-node representation of the EW2 and EW3 racks.

where

$$T_b = \int \rho c_p u T \, dy \Big/ \int \rho c_p u \, dy \tag{7}$$

At the outer boundary, the skin was assumed to exchange heat with the surroundings by both forced convection and radiation. For forced convection, it was assumed that the local heat transfer coefficient can be approximated by a correlation for a flat plate with an unheated starting section,[8] i.e.,

$$Nu_s = 0.0296 Re_s^{0.8} Pr^{0.33} [1 - (\xi/s)]^{-\frac{1}{9}} \tag{8}$$

Averaging the local heat transfer coefficient over the heated area, the average heat transfer coefficient may be written as

$$h_e = \int_{\xi}^{L} h_s \, ds \Big/ \int_{\xi}^{L} ds \tag{9}$$

The overall heat transfer coefficient between the inner and outer air may then be written as

$$U = 1 \Big/ \left[\frac{1}{h_i} + \frac{\Delta y_{\text{skin}}}{k_{\text{skin}}} + \frac{T_{\text{wo}} - T_a^*}{h_e \left(T_{\text{wo}} - T_a^*\right) - \alpha_s Q_s + \varepsilon_{\text{wo}} \left(T_{\text{wo}}^4 - T_\infty^4\right)} \right] \tag{10}$$

Figure 6 shows the heat transfer coefficient for the baffled section as a function of mass flow rate for the design point conditions.

The plot in Fig. 6 was fitted by the following equation and used in the network calculations:

$$U = (1.261) \mathring{m}^{0.6} \qquad (\text{Btu/h-ft}^2\text{-}^\circ\text{F}) \tag{11}$$

where $\mathring{m}$ is in pounds mass per minute per skin duct.

The variations in the overall heat transfer coefficient at 25,000-ft altitude are shown in Fig. 7. At the design flow rate of about 11

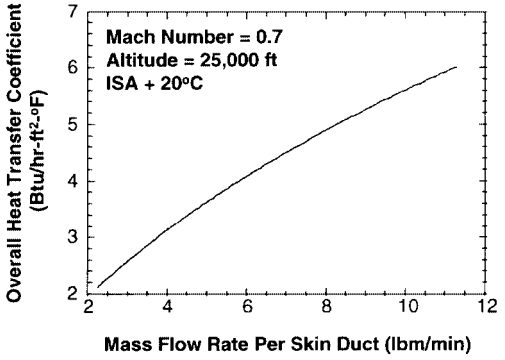

Fig. 6 Design point heat transfer coefficient in the baffled ducts.

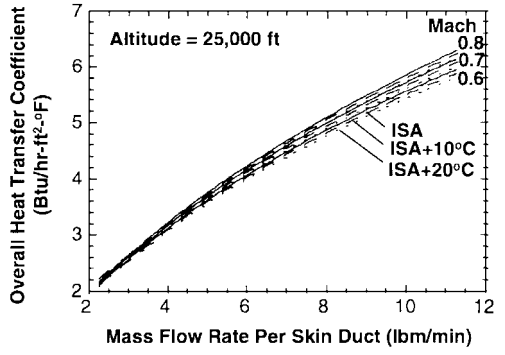

Fig. 7 Variations in the overall heat transfer coefficient at 25,000-ft altitude.

Table 1 Design point input parameters

Parameters	Values
Geometry	
Duct cross section	5 × 16 in.
Stringer height	0.85 in.
Stringer spacing	6 in.
Baseline baffle height	3 in.
Beginning of skin cooling	388 in. from the nose
End of skin cooling	477 in. from the nose
Materials	
Skin	ALCLAD 2024-T42
Inside	Anodized and coated with epoxy
Outside	Primer
Liner	Gray paint, perfect insulator
Outside conditions	
Flight altitude	25,000 ft
Mach number	0.7
Ambient temperature	ISA + 20°C (−14.5°C = 5.85°F)
Recovery temperature	46.8°F
Duct inside conditions	
Inlet temperature	122°F
Outlet pressure	10.9 psia (equiv. to 8000 ft.)
Flow rate	0–140 lbm/min (0–12.7 lbm/min per duct)
Coefficients	
Outside convective coefficient	25 Btu/ft^2-h-°F
Surface emissivity	0.8 (gray surface)
Surface solar absorptivity	0.8 ($\alpha_s/\varepsilon_{wo} = 1$)
Solar constant	430 Btu/ft^2-h

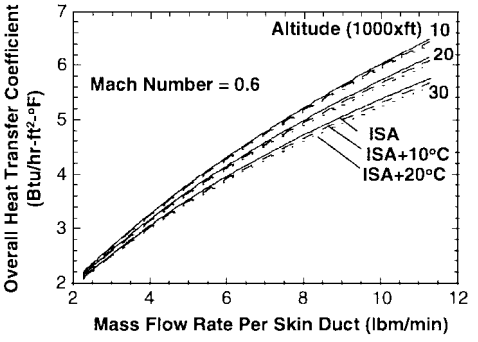

Fig. 8 Overall heat transfer coefficient for $M = 0.6$.

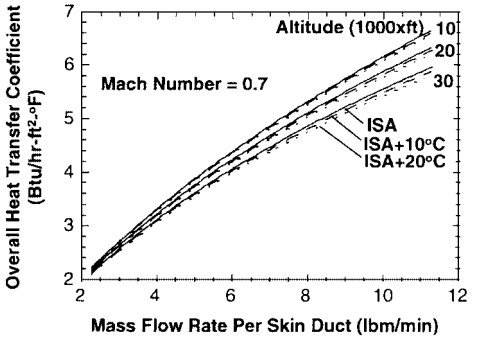

Fig. 9 Overall heat transfer coefficient for $M = 0.7$.

lbm/min, the maximum deviation of the overall heat transfer coefficient from the design point is about ±2%.

The design point input parameters are presented in Table 1.

The overall heat transfer coefficient for Mach numbers 0.6, 0.7, and 0.8 are shown in Figs. 8, 9, and 10, respectively. Figures 8–10 show the variations in the overall heat transfer coefficient as a function of mass flow rate for altitudes of 10,000, 20,000, and 30,000 ft, and temperatures of ISA, ISA +10°C, and ISA + 20°C.

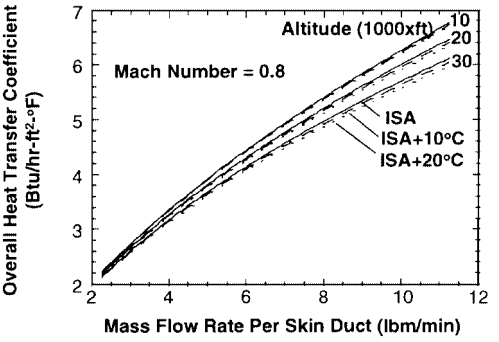

Fig. 10 Overall heat transfer coefficient for $M = 0.8$.

The plots in Figs. 8–10 were fitted by an equation of the following form and used in the network calculations:

$$U = C\dot{m}^n \tag{12}$$

The internal convective heat transfer coefficient in the ceiling plenum was determined from the following relationship:

$$Nu = 0.023 Re^{0.8} Pr^{0.33} \tag{13}$$

Because the controlling resistance to heat transfer in the ceiling plenum was the internal film coefficient, i.e., internal heat transfer coefficient, conduction through the skin and the external film resistance were neglected. The overall heat transfer coefficient was assumed to be approximately the same as the internal heat transfer coefficient using Eq. (13).

The heat transfer through the floor and aft bulkhead due to natural convection was also considered. For natural convective heat transfer at horizontal surfaces, the heat transfer coefficients were determined from

$$Nu = 0.14(GrPr)^{0.3} \tag{14}$$

and at vertical surfaces from

$$Nu = 0.1(GrPr)^{0.3} \tag{15}$$

Again, the internal heat transfer coefficient was used to approximate the overall heat transfer coefficient for the aft bulkhead and the floor surfaces. Heat transfer due to these surfaces is negligible.

Pressure Loss

The pressure distribution in the cooling system was analyzed using the network of nodes and links shown in Fig. 5. The difference in pressure between nodes is determined from the momentum equation (2).

The flow losses are associated with the third term of Eq. (2). Flow losses in each link are associated with viscous forces, i.e., friction, and nonideal flow through certain components. The latter losses occur in orifices, junctions, sudden expansions, and contractions, etc., and are generally due to flow separation and/or irreversible velocity head changes due to abrupt changes of flow channel area or flow direction. The losses may be expressed as

$$L(\dot{Q}_{ij}) = \tau_{\text{wall},ij}(\dot{Q}_{ij}) P_{ij} L_{ij} + \sum_{n=1}^{N} \frac{K \rho_{ij} \dot{Q}_{ij}^2}{2A_{ij}} \tag{16}$$

The shear stress τ_{wall} is generally expressed by the friction factor, defined by the Darcy equation,

$$f = 8\tau_{\text{wall}}/\rho v^2 \tag{17}$$

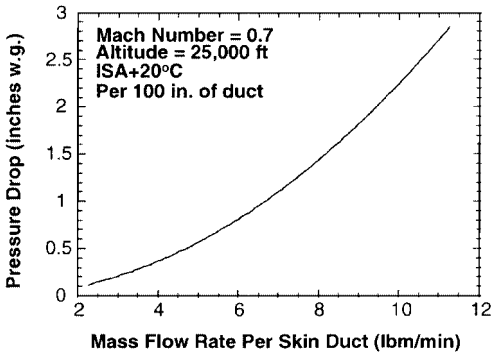

Fig. 11 Pressure drop in the baffled ducts.

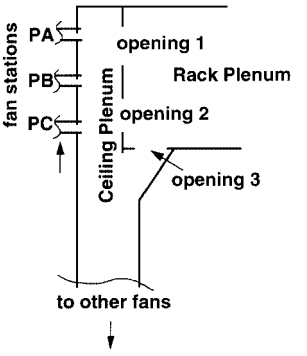

Fig. 12a Pressure loss model near the EW1 plenum exits.

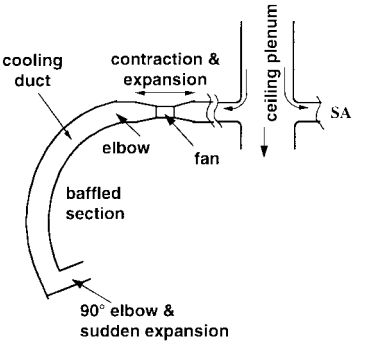

Fig. 12b Pressure loss model for flow distribution to the ducts.

Combining Eqs. (16) and (17) yields

$$L(\dot{Q}_{ij}) = \left(\frac{fL_{ij}}{De}\frac{\rho_{ij}\dot{Q}_{ij}^2}{2A_{ij}}\right) + \sum_{n=1}^{N}\frac{K\rho_{ij}\dot{Q}_{ij}^2}{2A_{ij}} \tag{18}$$

The viscous and minor losses in the various links were estimated using one of the following three methods.

Baffled Duct

The friction and minor losses in the baffled duct were determined as a function of mass flow rate by CFD analysis and are presented in Fig. 11.

The results in Fig. 11 were correlated by the following equations:

$$\Delta P/100\,\text{ft} = 0.022\mathring{m}^2 \qquad \text{[in. water gauge (in. w.g.)]} \tag{19}$$

where $\mathring{m}$ is in pounds mass per minute per skin duct, and

$$L_{\text{baffled duct}}(\dot{Q}_{ij}) = A_{ij}\mathring{m}^2 \tag{20}$$

Friction Losses

The friction losses in various sections of the plenum and ducting were calculated from the following equation:

$$L_{\text{friction}}(\dot{Q}_{ij}) = \frac{fL_{ij}}{D_e}\frac{\rho_{ij}\dot{Q}_{ij}^2}{2A_{ij}} \tag{21}$$

Values of f were obtained from the Moody chart for smooth ducts.

Minor Losses

Minor losses are customarily characterized by a K factor, as indicated in Eq. (16). K factors for a wide range of round and rectangular ducting components have been tabulated by Idelchik.[9] The K factors presented by Idelchick were calculated for our specific geometry and used in the network model. Figure 12 shows the main components of the cooling system for which the losses were calculated.

Because the MacroFlow analysis does not provide equivalent K factors for the viscous losses, they were estimated using the flow path dimensions and geometry. Whenever a velocity was required to estimate the flow losses, a total volumetric flow rate of 2100 ft^3/min and equal division of flow between the 11 cooling ducts was assumed. The following equation for the friction factor was used:

$$f = 0.11[(\varepsilon/D) + (68/Re)]^{0.25} \tag{22}$$

Equipment Losses

In addition to the three major sources of loss data just given, some prescribed K factors were also used to permit the flow rate in the chassis to adjust to the manufacturer's specifications. The analysis also uses specified loss data for the chassis, provided by the manufacturer in the form of quadratic analytical functions. For some of the rack components, the losses were provided by the component specification and were modeled quadratically. For certain rack chassis, where detailed data were not available, a K factor was assigned to analytically adjust the flow to its nominal value based on the manufacturer's specifications. The overall heat dissipation from and airflow through the equipment in the EW1 rack were experimentally verified.

Experimental Investigation

To characterize the thermal behavior of the chassis in the rack configuration, a replica of the rack/plenum configuration was constructed, and tests were performed to measure the overall heat dissipation and airflow rate. These tests were used to verify the manufacturers' specifications for EW1 chassis in the model.

The rack and plenum test setup is shown schematically in Fig. 13. The air enters the chassis from the front and exhausts into a plenum, which in turn exhausts into the environment. The shaded areas (Fig. 13a) indicate the air inlets to the individual equipment. Figure 13b shows the general layout of the equipment rack and plenum that was used to approximate the aircraft configuration. Major dimensions are indicated in Fig. 13b.

Thermocouples were used to measure the inlet and outlet temperatures of each chassis and the bulk temperature at the rack and plenum exits. The air pressure in the plenum was measured by a Dwyer Model 400 inclined manometer. The plenum exit velocity was measured at nine locations in each of the three exit openings using an Alnor Velometer Series 6000 air velocity meter with a diffuser probe. The Velometer was verified by comparison with pitot tube measurements of the velocity of air leaving a 2-in. pipe.

The airflow direction through the system is from the front of the schematic through the instruments (not shown in Fig. 13b) to the rack plenum at the back of the rack, then vertically upward to the upper portion of the rack plenum, then out to the ceiling plenum through the openings indicated in the upper part of the rack plenum at the top left of Fig. 13b.

Tests indicated that, at room conditions, the overall flow rate through the rack was 2100 ft^3/min ($\pm$200 ft^3/min) and, for a plenum exit area of 1.92 ft^2, the pressure in the plenum was 0.15 in. w.g. ($\pm$0.02 in. w.g.). The temperature rise through the rack was 10°C ($\pm$1°C. This yields a heat dissipation of 11 $\pm$ 1 kW, which is consistent with the manufacturer's specifications of 2029 ft^3/min and 10.7 kW (Refs. 1 and 5).

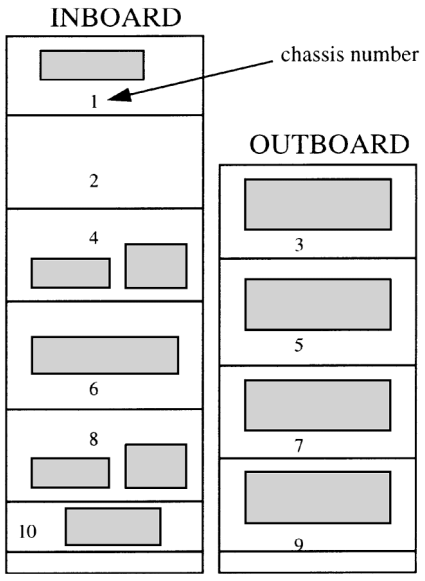

Fig. 13a Schematic of front view of EW1 rack.

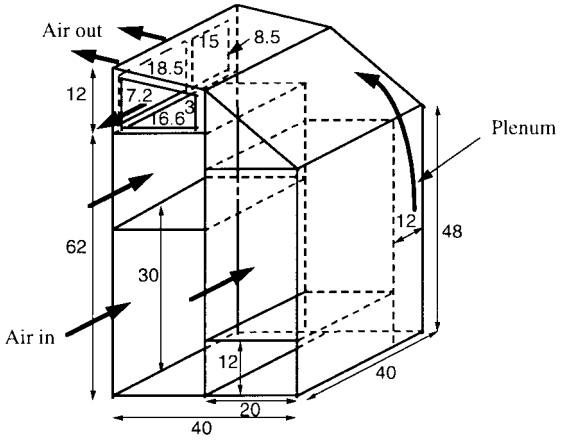

Fig. 13b Schematic of EW1 rack and plenum (dimensions in inches).

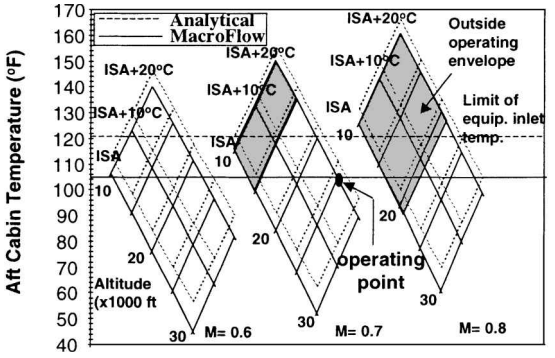

Fig. 14 Aft cabin temperature.

Model Predictions

Solid lines in Fig. 14 show the aft cabin average temperature for the flight envelope as a function of Mach number, i.e., the speed of the aircraft, flight altitude, and ambient temperature, i.e., ISA–ISA + 20°C. For example, for an aircraft flying at 25,000 ft at Mach 0.7 on an ISA + 20°C day, the predicted cabin temperature is about 105°F. The current operating point is designated with a dot on Fig. 14. This point is below the maximum inlet temperature for the equipment, which is presently defined as 122°F (40°C). The shaded regions on the graph are outside the aircraft's operating envelope.

Dotted lines in Fig. 14 show the results of the analytical predictions.[1–3] Aft cabin temperatures predicted using MacroFlow

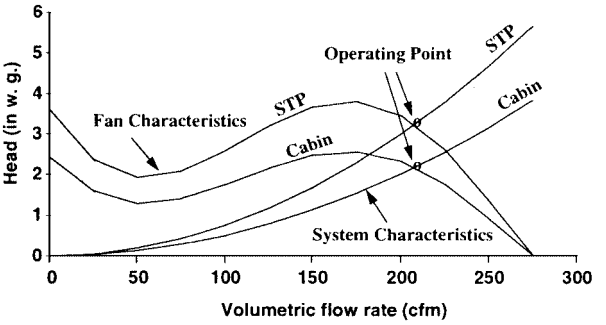

Fig. 15 Single ceiling fan performance.

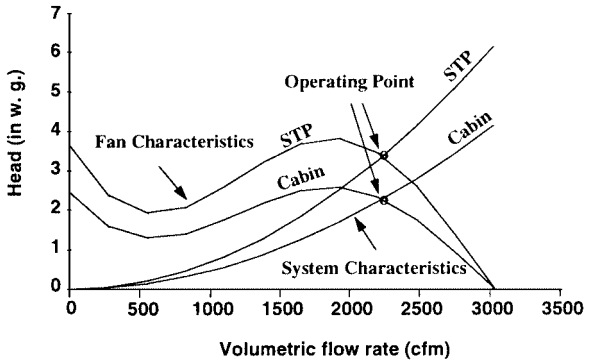

Fig. 16 Combined ceiling fans performance (11 fans).

are lower than the analytical results presented by Dyson et al.[1] and Hashemi et al.[2,3] This is mainly due to higher recirculation airflow through the EW1 rack (2400 vs 2100 ft^3/min), which is a result of coupling between the ceiling fans and the chassis fans.

The pressure distribution through the cooling system was calculated using the design point parameters. Then, using the pressure drop along a typical run and the ceiling fan performance curve, the fan operating point was estimated. This is shown in Fig. 15. Figure 15 shows that, for a total flow rate of about 2400 ft^3/min divided equally between 11 ducts (190 ft^3/min per duct), the pressure head to overcome by the fan is about 2 in. of H_2O, which satisfies the model requirements. It is noted that this is in very good agreement with the analytical calculations for the overall pressure drop.

Figure 15 also shows the operating curves of the fan at STP conditions. The fan scaling laws were used to determine the fan performance at STP from the cabin conditions. The operating points at STP and cabin pressure lie at the intersection of the fan performance and system pressure-loss characteristics.

Using series fan laws, i.e., same static head, additive volumetric head, the combined performance of the 11 fans in the aft cabin was evaluated. Figure 16 shows the operating point of the fans at STP and cabin conditions. For approximately 2 in. w.g. pressure drop in each leg of the system at cabin conditions, a total volumetric flow rate of about 2400 ft^3/min is obtained. This confirms the consistency between the flow rate and pressure drop predicted by MacroFlow.

Conclusions

A network model has been developed to characterize airflow and temperature distribution in the aft cabin. This model was designed to predict the performance of the supplementary cooling system. Using the current design parameters, the model indicates that the aft cabin temperature will be approximately 105°F, which is nearly the same as the design goal of 104°F (see Fig. 14).

This cabin temperature is lower than that presented by Dyson et al.[1] and Hashemi et al.[2,3] because of a higher recirculation flow rate in the aft cabin. The higher recirculation flow is due to coupling between the ceiling and the equipment fans. The inherent assumption in these results is that the higher flow rate can be achieved through bypass openings in the rack and plenum.

Because several hundred theoretical design parameters, and at times only best guesses, were used as input to the network model, the predictions should be considered preliminary and used judiciously. However, it should be noted that the overall energy balance and aft cabin temperature predictions are remarkably consistent with our analytical models and engineering calculations. The recirculation flow is a function of pressure drop in the system, which will ultimately be determined by the as-built system ducting and actual fan performances. However, note that the network model predictions for the overall airflow agree with previous engineering calculations.[3]

A series of tests was performed to design a low-impedance plenum for the EW1 rack. The nominal design produced a flow rate of 2100 ft^3/min ($\pm$200 ft^3/min) and a pressure rise of 0.15 in. w.g. ($\pm$0.02 in. w.g.) at room conditions, which was judged to be satisfactory. The temperature rise through the rack was 10°C ($\pm$1°C). This combination of flow rate and temperature rise yields a heat dissipation of 11 $\pm$ 1 kW, which is consistent with specifications of 2029 ft^3/min, and 10.7 kW.

References

[1]Dyson, E., Hashemi, A., and Wong, H., "High-Power Electronics Heat Rejection from Aircraft Skin," *Journal of Enhanced Heat Transfer*, Vol. 3, No. 3, 1996, pp. 165–176.

[2]Hashemi, A., Dyson, E., and Wong, H., "Cooling of Onboard High-Power Electronics Using Augmented Heat Rejection from Aircraft Skin," *Proceedings of the Symposium on Thermal Science and Engineering in Honor of Chancellor Chang-Lin Tien*, edited by R. O. Buckius, Office of Printing Services, Univ. of Illinois, Urbana–Champaign, IL, 1995, pp. 465–474.

[3]Hashemi, A., Dyson, E., and Wong, F., "EST Challenger Supplementary Cooling Installation: Analytical and Experimental Investigations," Lockheed Martin Missiles and Space, Rept. LMMS/P430563, Palo Alto, CA, May 1995.

[4]Hashemi, A., Wong, F., and Dyson, E., "EST Challenger Skin Cooling: Fluid Flow and Heat Transfer," Lockheed Martin Missiles and Space, Rept. LMSC/P108691, Palo Alto, CA, July 1994.

[5]Hashemi, A., Dyson, E., and Glassford, P., "EST Challenger Supplementary Cooling: System Network Model and Equipment Performance," Lockheed Martin Missiles and Space, Rept. LMMS/P421018, Palo Alto, CA, Nov. 1995.

[6]"MacroFlow, A Computer Program for Network Analysis of Complex Systems," Innovative Research, Inc., Minneapolis, MN, 1995.

[7]Patankar, S.V., *Numerical Heat Transfer and Fluid Flow*, McGraw–Hill, New York, 1980.

[8]Incropera, F. P., and Dewitt, D. P., *Fundamentals of Heat and Mass Transfer*, 3rd ed., Wiley, New York, 1990.

[9]Idelchik, I. E., *Handbook of Hydraulic Resistance*, 3rd ed., CRC Press, Boca Raton, FL, 1994.